Article

Diffusion-Based Deprotection in Mesoporous Materials: A Strategy for Differential Functionalization of Porous Silica Particles

Kai Cheng, and Christopher C. Landry

J. Am. Chem. Soc., **2007**, 129 (31), 9674-9685• DOI: 10.1021/ja070598b • Publication Date (Web): 18 July 2007

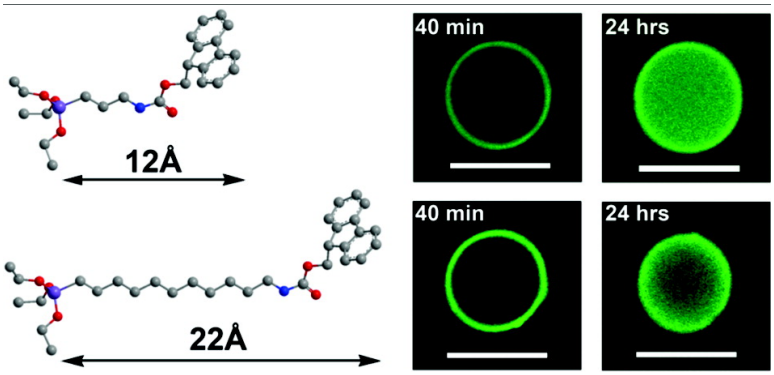

More About This Article

Additional resources and features associated with this article are available within the HTML version:

- Supporting Information
- Links to the 9 articles that cite this article, as of the time of this article download
- Access to high resolution figures
- Links to articles and content related to this article
- Copyright permission to reproduce figures and/or text from this article

View the Full Text HTML

J|A|C|S
ARTICLES
Published on Web 07/18/2007

Diffusion-Based Deprotection in Mesoporous Materials: A Strategy for Differential Functionalization of Porous Silica Particles

Kai Cheng and Christopher C. Landry*

Contribution from the Department of Chemistry, 82 University Place, University of Vermont, Burlington, Vermont 05405

Received January 26, 2007; E-mail: christopher.landry@uvm.edu

Abstract: A monodisperse, spherical mesoporous silica (Acid-Prepared Mesoporous Spheres, APMS) was prepared and then functionalized with two types of Fmoc (9-fluorenylmethyloxycarbonyl) terminated silanes with variable chain lengths. N_2 physisorption experiments indicated that, under some conditions, the pores of the solid were completely filled by the Fmoc-protected organosilanes. These blocked pores were then "reopened" by the cleavage of Fmoc groups with a piperidine solution. In contrast to the solution reaction, this deprotection reaction was much slower within the pores. The rate of deprotection was followed by UV/visible spectroscopy, and a plot of Fmoc released versus time showed a sigmoidal shape. An empirical model was applied to the data, which indicated that the reaction was influenced by the concentration and temperature of the piperidine solution as well as the number of Fmoc moieties within the pores. Using this information, we show that the location of the deprotection reaction in the pores of the silica can be empirically controlled. Our work provides a method by which the surface of the porous silica can be functionalized in a well-defined manner. This method can be used to produce materials for catalysis or drug delivery.

Introduction

The synthesis and modification of mesoporous silica have recently received much attention,[1−7] due to its large internal surface area and pore volume, tunable and narrowly distributed pore diameter, controllable surface functionalization, chemical inertness, and biocompatibility, all of which has made it ideal for use in biomedical applications such as biocatalysis,[8−10] separation and decontamination,[11] affinity chromatography,[12−15] and drug delivery.[16] The successful use of porous solids in these applications often requires different surface properties of the internal (pore) and external surfaces. For example, chemical functionalization of the internal pore surfaces with proper functional groups is one way to trap various molecules with different sizes and functionalities inside the pores.[17−19] The external particle surfaces can then be modified in a different manner to provide enhanced biocompatibility, dispersion, or other properties. The key issue is that chemical modification of the external surface should not only confer the desired function but also leave the internal pore volume available to carry exchangeable molecules or perform a separate function.

Mesoporous silica is synthesized by polymerizing a silica source in the presence of a surfactant template. The pores of the solid are created by either calcination of the resulting organic−inorganic composite in air or surfactant extraction. Postsynthesis grafting and co-condensation by adding an organosilane to the synthesis mixture are two popular strategies for immobilization of functional groups onto mesoporous silica via covalent bonds.[20] Although co-condensation provides a more homogeneous distribution of the functional groups within the silica than postsynthesis grafting, incomplete attachment and phase separation during the synthetic process can make it more difficult to quantitatively control the loadings of functional groups.[21,22] Another method involving simultaneous extraction of the surfactant (which is used to create the mesopores during

(1) Kresge, C. T.; Leonowicz, M. E.; Roth, W. J.; Vartuli, J. C.; Beck, J. S. *Nature* **1992**, *359*, 710.
(2) Corma, A. *Chem. Rev.* **1997**, *97*, 2373.
(3) Beck, J. S.; Vartuli, J. C.; Roth, W. J.; Leonowicz, M. E.; Kresge, C. T.; Schmitt, K. D.; Chu, C. T.-W.; Olson, D. J.; Sheppard, E. W.; McCullen, S. B.; Higgins, J. B.; Schlenker, J. L. *J. Am. Chem. Soc.* **1992**, *114*, 10834.
(4) Gallis, K. W.; Araujo, J. T.; Duff, K. J.; Moore, J. G.; Landry, C. C. *Adv. Mater.* **1999**, *11*, 1452.
(5) Gallis, K. W.; KEklund, A. G.; Jull, S. T.; Araujo, J. T.; Moore, J. G.; Landry, C. C. *Stud. Surf. Sci. Catal.* **2000**, *129*, 747.
(6) Nassivera, T. W.; Eklund, A. G.; Landry, C. C. *J. Chromatogr. A* **2002**, *973*, 97.
(7) Sorensen, A. C.; Fuller, B. L.; Eklund, A. G.; Landry, C. C. *Chem. Mater.* **2004**, *16*, 2157.
(8) Bornscheuer, U. T. *Angew. Chem., Int. Ed.* **2003**, *42*, 3336.
(9) Cetinus, S. A.; Oztop, H. N. *Enzyme Microb. Technol.* **2003**, *32*, 889.
(10) Lei, C.; Shin, Y.; Liu, J.; Ackerman, E. J. *J. Am. Chem. Soc.* **2002**, *124*, 11242.
(11) Wang, Y.; Caruso, F. *Chem. Mater.* **2005**, *17*, 953.
(12) Lakhiari, H.; Legendre, E.; Muller, D.; Jozefonvicz, J. *J. Chromatogr. B* **1995**, *664*, 163.
(13) Schiel, J. E.; Mallik, R.; Soman, S.; Joseph, K. S.; Hage, D. S. *J. Sep. Sci.* **2006**, *29*, 719.
(14) Hage, D. S. *Clin. Chem.* **1999**, *45*, 593.
(15) Svec, F. *J. Sep. Sci.* **2005**, *28*, 729.
(16) Lai, C.-Y.; Trewyn, B. G.; Jeftinija, D. M.; Jeftinija, K.; Xu, S.; Jeftinija, S.; Lin, V. S.-Y. *J. Am. Chem. Soc.* **2003**, *125*, 4451.
(17) Stein, A.; Melde, B. J.; Schroden, R. C. *Adv. Mater.* **2000**, *12*, 1403.
(18) Hoffmann, F.; Cornelius, M.; Morell, J.; Froba, M. *Angew. Chem., Int. Ed.* **2006**, *45*, 3216.
(19) Descalzo, A. B.; Martinez-Manez, R.; Sancenon, R.; Hoffmann, K.; Rurack, K. *Angew. Chem., Int. Ed.* **2006**, *45*, 5924.
(20) Vinu, A.; Hossain, K. Z.; Ariga, K. *J. Nanosci. Nanotechnol.* **2005**, *5*, 347.
(21) Liu, Y.-H.; Lin, H.-P.; Mou, C.-Y. *Langmuir* **2004**, *20*, 3231.
(22) Huh, S.; Wiench, J. W.; Yoo, J.-C.; Pruski, M.; Lin, V. S.-Y. *Chem. Mater.* **2003**, *15*, 4247.

10.1021/ja070598b CCC: $37.00

synthesis) and grafting of organic functionalities successfully provided very well-defined surface functionization.[21] However, all of these methods result in the modification of both interior and exterior surfaces of mesoporous silicas. Grafting of silane groups *before* the extraction of the surfactant has been used to exclusively modify the exterior particle surface.[23] For mesoporous silicas synthesized under acidic conditions, however, the surfactant−silane exchange process cannot be ignored since the surfactants are not strongly attracted to the silica. This results in unexpected modification within the pores.[21] We noticed that reactions within the pores are spatially confined and the diffusion of reactant and product molecules is physically constrained. This produces a molecular size-exclusion effect,[6] which can be used to control chemical reactions. We reasoned that this size-exclusion effect could be exploited in combination with established protection/deprotection methods to produce a mesoporous silica sphere with amine groups exposed solely on its external surface, which could then be used to covalently bind peptides or other biomolecules to the external surface. The internal pore volume could then be opened by complete deprotection. Protection/deprotection of surface-bound amines was selected because it is a well-known reaction, and the resulting materials are potentially useful. Here, we studied the rates of diffusion and reaction in the modified mesoporous silica spheres with UV−visible spectroscopy and confocal fluorescence microscopy. An empirical equation can be used to model the experimental data in order to understand the mechanism of deprotection within the pores.[24]

Experimental Section

Materials and Methods. ^{1}H and ^{13}C NMR spectra were recorded on a Bruker ARX-500 NMR spectrometer operating at 500 and 125 MHz, respectively. $CDCl_3$ was used as the solvent and also served as an internal reference. ^{29}Si solid-state MAS NMR experiments were obtained on the same instrument at a frequency of 79.5 MHz, and chemical shifts were referenced to 3-(trimethylsilyl)-1-propanesulfonic acid sodium salt. Samples were spun at 4 kHz, and a 30 s recycle delay was used. Mass spectra were measured using a Finnegan 4610 spectrometer. FTIR spectra were obtained on a Perkin-Elmer 2000 FTIR spectrometer. Compressed KBr pellets containing about 2 wt % of sample were used for these studies. Thermogravimetric analysis (TGA) was performed on a Perkin-Elmer Pyris 1 DSC-TGA. Scans were performed between 25 and 800 °C at 5 °C/min. UV−visible spectra between 200 and 850 nm were obtained using an Ocean Optics S2000 multichannel fiber optic spectrophotometer system. Powder X-ray diffraction (XRD) experiments were performed on a Scintag X1 $\theta-\theta$ diffractometer equipped with a Peltier (solid-state thermoelectrically cooled) detector using Cu Kα radiation. N_2 physisorption isotherms were obtained on a Micromeritics ASAP 2010 instrument. Samples were degassed at 110 °C under vacuum overnight prior to measurement. Surface areas were measured using the BET method, pore size distributions were calculated from the BJH method,[25,26] and the total pore volumes were calculated from the nitrogen adsorption/desorption data (single-point volume at $p/p_0 = 0.995$). Fluorescence confocal scanning laser microscopy (CSLM) was performed using a BioRad MRC 1024ES confocal laser scanning imaging system. Dye fluorescence was measured at 488 nm, and a 60× oil-immersion lens was used to image the samples. Calcinations were carried out in a box furnace under conditions of flowing air. The following heating profile was used for calcinations: 2 °C/min ramp to 450°C, 240 min hold at 450 °C, 10 °C/min ramp to 550 °C, 480 min hold at 550 °C. Parr autoclaves were purchased from the Parr instrument Corporation.

N-(9-Fluorenylmethyloxycarbonyl)oxysuccinimide (Fmoc-OSu) was obtained from Advanced Chem Tech. Alexa Fluor 488 carboxylic acid, succinimidyl ester was obtained from Molecular Probes. Concentrated HCl was obtained from J. T. Baker. All other chemicals were obtained from Aldrich. Triethylamine (Et_3N), hexane, toluene, and methylene chloride (CH_2Cl_2) were distilled prior to use, and acetonitrile (MeCN) was stored over molecular sieves. Other solvents and chemicals were used as received.

Synthesis of (3-Triethoxysilylpropyl)carbamic Acid 9*H*-Fluorenylmethyl Ester (Fmoc-APTES). A solution of aminopropyltriethoxysilane, APTES (4.68 mL, 20.0 mmol), in 100 mL of anhydrous CH_2Cl_2 was prepared and cooled in an ice bath. In a separate flask, *N*-(9-fluorenylmethyloxycarbonyl)oxysuccinimide, Fmoc-OSu (6.88 g, 20.4 mmol), was dissolved in a small amount of anhydrous CH_2Cl_2; this solution was then slowly added to the APTES solution with stirring. After 2 h, rotary evaporation of the solvent left an oily white product which was purified by flash chromatography with ethyl acetate/hexane (1:4) to yield the product (7.8 g, 17.6 mmol, 88% yield) as a white solid. ^{1}H NMR (500 MHz, $CDCl_3$): δ 7.77 (2H, d, $J = 7.5$ Hz, Ar−H), 7.60 (2H, d, $J = 7.6$ Hz, Ar−H), 7.40 (2H, t, $J = 7.5$ Hz, Ar−H), 7.31 (2H, t, $J = 7.6$ Hz, Ar−H), 5.03 (1H, broad s, NH), 4.40 (2H, d, $J = 6.86$ Hz, $COOCH_2$), 4.22 (1H, t, $J = 6.18$ Hz, Ar−CH), 3.823 (6H, q, $J = 7.00$ Hz, $SiOCH_2$), 3.208 (2H, q, $J = 6.09$ Hz, $NHCH_2$), 1.65 (2H, quint, $J = 6.90$ Hz, CH2), 1.23 (9H, t, $J = 7.00$ Hz, CH_3), 0.643 (2H, t, $J = 8.05$ Hz, $SiCH_2$). ^{13}C NMR (125 MHz, $CDCl_3$): δ 156.6, 144.2, 141.5, 127.8, 127.2, 125.2, 120.1, 66.6, 58.6, 47.5, 43.6, 23.4, 18.5, 7.8. ES−MS: calcd for ($M + H^+$) $C_{24}H_{34}NO_5Si$ 444.2, found 444.3.

Synthesis of ω-Undecenamide. A mixture of urea (15 g, 0.25 mol) and undecylenic acid (23.01 g, 0.125 mol) was placed in a round-bottomed flask fitted with a condenser. The mixture was heated to 170−180 °C for 4 h and then allowed to cool. When the temperature had dropped to 110−120 °C, a Na_2CO_3 solution (5%, 100−150 mL) was carefully added through the condenser to stop the reaction. The mixture was then cooled in an ice bath, and the product was collected by filtration. The crude material was recrystallized in 95% EtOH at least twice. The final product was dried in vacuo to give an almost colorless solid (14.5 g, 79.1 mmol, 63% yield). ^{1}H NMR (500 MHz, $CDCl_3$): δ 5.81 (1H, ddt, $J = 16.9$, 10.2, 6.8 Hz, CH_2═CH), 5.27 (2H, broad, NH_2), 4.91−5.01 (2H, m, CH_2═CH), 2.22 (2H, t, $J = 7.5$ Hz, $COCH_2$), 2.04 (2H, q, $J = 7.1$ Hz, CH_2═$CHCH_2$), 1.642 (2H, quint, $J = 7.5$ Hz, $COCH_2CH_2$), 1.30−1.39 (12H, m, alkyl-*H*).

Synthesis of 11-Undecenylamine. $LiAlH_4$ (2.3 g, 60.6 mmol) was placed in a 250 mL round-bottom flask containing 50 mL of anhydrous THF, and the mixture was heated at reflux for 30 min under N_2. After this time, heating was stopped and a solution of undecenamide (5.0 g, 27.3 mmol) in 100 mL of anhydrous THF was introduced with stirring. Reflux was continued under N_2 with stirring for an additional 24 h, and the reaction was then quenched by dropwise addition of 8 mL of water to destroy excess $LiAlH_4$. The resulting white precipitate was removed by filtration and washed with 3 × 15 mL EtOAc. After the combined organic phases were dried over anhydrous Na_2SO_4, evaporation of the solvent followed by vacuum distillation (40 ∼ 50 °C at 0.06 Torr) gave the product as a colorless oil (3.25 g, 19.2 mmol, 70% yield). ^{1}H NMR (500 MHz, $CDCl_3$): δ 5.81 (1H, ddt, $J = 16.9$, 10.2, 6.8 Hz, CH_2═CH), 4.91−5.01 (2H, m, CH_2═CH), 2.67 (2H, t, $J = 7.0$ Hz, NH_2CH_2), 2.03 (2H, q, $J = 7.2$ Hz, CH_2═$CHCH_2$), 1.28−1.44 (14H, m, alkyl-*H*), 1.02 (2H, broad s, NH_2).

Synthesis of (9*H*-Fluoren-9-yl)methyl Undec-10-enylcarbamate (Fmoc-11-Aminoundecene). A solution of 11-undecenylamine (0.677 g, 4 mmol) in 30 mL of anhydrous CH_2Cl_2 was prepared and cooled

(23) Mal, N.-K.; Fujiwara, M.; Tanaka, Y. N. *Nature* **2003**, *421*, 350.
(24) Giraldo, J.; Vivas, N. M.; Vila, E.; Badia, A. *Pharmacol. Ther.* **2002**, *95*, 21.
(25) Brunauer, S. *The Adsorption of Gases and Vapors*; Princeton University Press: Princeton, NJ, 1943.
(26) Webb, P. A.; Orr, C. *Analytical Methods in Fine Particle Technology*; Micromeritics Instrument Corporation: Norcross, GA, 1997.

in an ice bath. In a separate flask, *N*-(9-fluorenylmethyloxycarbonyl)-oxysuccinimide, Fmoc-OSu (1.417 g, 4.2 mmol), was dissolved in a small amount of anhydrous CH_2Cl_2; this solution was then slowly added to the APTES solution with stirring. After 2 h, rotary evaporation of the solvent left an oily white product which was purified by flash chromatography on silica gel with ethyl acetate/hexane (1:4) to yield the product as a white solid (1.42 g, 3.63 mmol, 91% yield). ^{1}H NMR (500 MHz, $CDCl_3$): δ 7.77 (2H, d, J = 7.5 Hz, Ar—H), 7.60 (2H, d, J = 7.6 Hz, Ar—H), 7.40 (2H, t, J = 7.5 Hz, Ar—H), 7.31 (2H, t, J = 7.6 Hz, Ar—H), 5.81 (1H, ddt, J = 16.9, 10.2, 6.8 Hz, CH_2═CH), 4.91−5.01 (2H, m, CH_2═CH), 4.70 (1H, broad s, NH), 4.41 (2H, d, J = 6.7 Hz, $COOCH_2$), 4.22 (1H, t, J = 6.18 Hz, Ar—CH), 3.18 (2H, m, NH—CH_2), 2.04 (2H, q, J = 7.0 Hz, CH_2═$CHCH_2$), 1.29−1.38 (14H, m, alkyl-*H*).

Synthesis of (9*H*-Fluoren-9-yl)methyl 11-(Triethoxysilyl)undecylcarbamate (Fmoc-AUTES). After bubbling dry N_2 into 20 mL of a dry dichloromethane solution of Fmoc-11-aminoundecene (0.714 g, 1.82 mmol) and triethoxysilane (0.3286 g, 0.367 mL, 2.0 mmol) for 10 min, 0.2 μmol of Pt(dvs), platinum(0)-1,3-divinyl-1,1,3,3,-tetramethyldisiloxane complex, 3 wt % in xylenes (15 μL) was added and the resulting mixture was refluxed for 12 h. After removing the solvent under reduced pressure, an oily white product was obtained which was further purified by flash chromatography with ethyl acetate/hexane (1:4) to yield the product as a white solid (0.85 g, 1.53 mmol, 84% yield). ^{1}H NMR (500 MHz, $CDCl_3$): δ 7.77 (2H, d, J = 7.5 Hz, Ar—H), 7.60 (2H, d, J = 7.6 Hz, Ar—H), 7.40 (2H, t, J = 7.5 Hz, Ar—H), 7.31 (2H, t, J = 7.6 Hz, Ar—H), 4.74 (1H, broad s, NH), 4.41 (2H, d, J = 6.6 Hz, $COOCH_2$), 4.22 (1H, t, J = 6.46 Hz, Ar—CH), 3.82 (6H, q, J = 7.00 Hz, $SiOCH_2$), 3.19 (2H, q, J = 5.8 Hz, $NHCH_2$), 1.65−1.22 (14H, m, alkyl-*H*), 0.636 (2H, t, J = 8.2 Hz, $SiCH_2$). ^{13}C NMR (125 MHz, $CDCl_3$): δ 156.6, 144.2, 141.5, 127.8, 127.2, 125.2, 120.1, 66.6, 58.5, 47.5, 41.3, 32.8, 30.2−29.5, 29.3, 26.9, 22.9, 18.5, 14.3, 10.6. ES−MS: calcd for ($M + H^+$) $C_{32}H_{50}NO_5Si$ 556.34, found 557.1.

Synthesis of APMS. Cetyltrimethylammonium bromide (1.20 g, 3.29 mmol) and concentrated HCl (4.5 g, 36.5 wt %, 45.0 mmol) were added to distilled water (55.5 g) and stirred rapidly until the surfactant had dissolved. Tetraethoxysilane (5.65 g, 27.1 mmol) was then added, and the mixture was stirred at room temperature for 1 h. The mixture was then transferred to a Teflon-lined Parr autoclave and heated at 150 °C for 40 min. The mixture was then cooled to room temperature, and the resulting white precipitate was collected by filtration, air-dried, and calcined (1.10 g).

Synthesis of Functionalized Silica. A calcined sample of either APMS or Nucleosil (0.60 g) was suspended in 20 mL of dry toluene in a dry, inert atmosphere. A solution of organosilane (0.1−5 mmol) dissolved in 5 mL of dry toluene was then added, and the mixture was refluxed at 110 °C for 24 h. After the mixture was cooled to room temperature, the white powder was recovered by filtration, air-dried, and then vacuum-dried for 24 h prior to further use.

Quantitation of Organic Loading on APMS by UV−visible Spectrophotometry. In a typical analysis, silica-Fmoc (4.0 mg) and NH_4F (15.0 mg) were placed in a plastic vial. After rapid addition of concentrated HCl (120 μL), the mixture was incubated at 50 °C for 30 min with continuous vortexing. Distilled water (0.5 mL) was then added, and the remaining organic components were extracted with CH_2Cl_2 (5 × 1 mL). After dilution to 10 mL with additional CH_2Cl_2, the absorbance of Fmoc-adduct in the extractant was determined at 289 nm using UV−visible spectroscopy, using a calibration curve that was prepared using standard amounts of Fmoc-APTES.[27] Samples were assayed in triplicate.

Kinetic Study of the Deprotection Reaction of Silica-Fmoc. Kinetic studies were performed in a 100 mL round-bottom flask with a double-layer water jacket connected to a Brinkman Lauda (Model RMS6) recirculating unit, which provided precise temperature control, to within 0.01 °C. A solution of piperidine in DMF (2 to 40%, 50 mL total volume) was thermally equilibrated at a temperature of 25, 30, or 40 °C for 30 min. Organosilane-modified silica (100.0 mg) was quickly added to this solution, and the deprotection was carried out for 24 h. Aliquots of the mixture (500 μL) were removed from the deprotection mixture at predetermined time intervals. The supernatant was obtained by centrifugation, and the absorption of the collected supernatants at 289 nm was monitored with UV/visible spectroscopy using a quartz cell with a 10 mm path length. The amount of Fmoc-piperidine adduct in the solution was obtained from a calibration curve measured with a series of different, known Fmoc-APTES solutions that had been treated under the same conditions.

Attachment of Fluorescent Dye to Free Amines of Deprotected Silica-Fmoc. Deprotected silica-Fmoc samples (2.0 mg) were suspended in 200 μL of a 100 mM $NaHCO_3$ solution. The suspensions were then transferred to vials containing Alexa Fluor 488 carboxylic acid, succinimidyl ester (10 μg, 0.0155 μmol). After incubation for 4 h at room temperature and 12 h at 4 °C with continuous shaking, the samples were recovered by centrifugation, washed successively with a 100 mM $NaHCO_3$ solution, distilled water, and MeOH, and then air-dried and stored at 4 °C in the dark. The procedure could also be used at any stage of the silica modification to locate free amines within the samples.

Results and Discussion

Acid-Prepared Mesoporous Spheres (APMS) were used in this study. They are easily and rapidly synthesized, have pores with an average diameter of 30 Å, and have a 5 μm particle diameter.[4−7,28] They were chosen for this study because of their monodisperse, spherical particle morphology, which was easily recognized by microscopy.[4,5,28] The postsynthesis grafting procedure was used to immobilize functionalized amines on APMS through covalent linkages between organic molecules and silanol groups.[29−35] The degree of functionalization and the distribution of functional groups were influenced by the densities of surface silanol groups (Si−OH) on the mesoporous silica wall, the reactivities of the organosilanes, and their accessibility to surface silanols. The physical properties of the surface-functionalized APMS were characterized using X-ray diffraction (XRD), ^{29}Si MAS NMR spectrometry, FT-IR spectroscopy, and thermogravimetric analysis (TGA).

The removal of the Fmoc group was usually achieved by treatment with piperidine in *N*,*N*′-dimethylformamide (DMF).[36] The mechanism of the Fmoc-deprotection reaction involves the formation of aromatic cyclopentadiene intermediates, which are rapidly eliminated to form dibenzofulvene, which is further scavenged by piperidine to form the Fmoc-adduct 1-((9*H*-fluoren-9-yl)methyl) piperidine. This product strongly absorbs UV radiation at 289 nm, offering the potential to monitor the deprotection reaction by UV/visible spectroscopy. Because the deprotection reactions occurred within the confined space of the pore network, the reaction rates were significantly different from those in solution. The concentration and temperature of

(27) See the Supporting Information.

(28) Gallis, K. W.; Landry, C. C. U.S. Patent 6,334,988, 2002.
(29) Zhao, X. S.; Lu, G. Q. *J. Phys. Chem. B* **1998**, *102*, 1556.
(30) Jal, P. K.; Patel, S.; Mishra, B. K. *Talanta* **2004**, *62*, 1005.
(31) De Juan, F.; Ruiz-Hitzky, E. *Adv. Mater.* **2000**, *12*, 430.
(32) Feng, X.; Fryxell, G. E.; Wang, L.-Q.; Kim, A. Y.; Liu, J.; Kemner, K. M. *Science* **1997**, *276*, 923.
(33) Lim, M. H.; Stein, A. *Chem. Mater.* **1999**, *11*, 3285.
(34) Liu, J.; Shin, Y.; Nie, Z.; Chang, J. H.; Wang, L.-Q.; Fryxell, G. E.; Samuels, W. D.; Exarhos, G. J. *J. Phys. Chem. A* **2000**, *104*, 8328.
(35) Lindner, E.; Schmneller, T.; Auer, F.; Mayer, H. A. *Angew. Chem., Int. Ed.* **1999**, *38*, 2154.
(36) Atherton, E.; Sheppard, R. C. *The Peptides* **1987**, *9*, 1.

Scheme 1. Syntheses of Organosilanes Used in This Study[a]

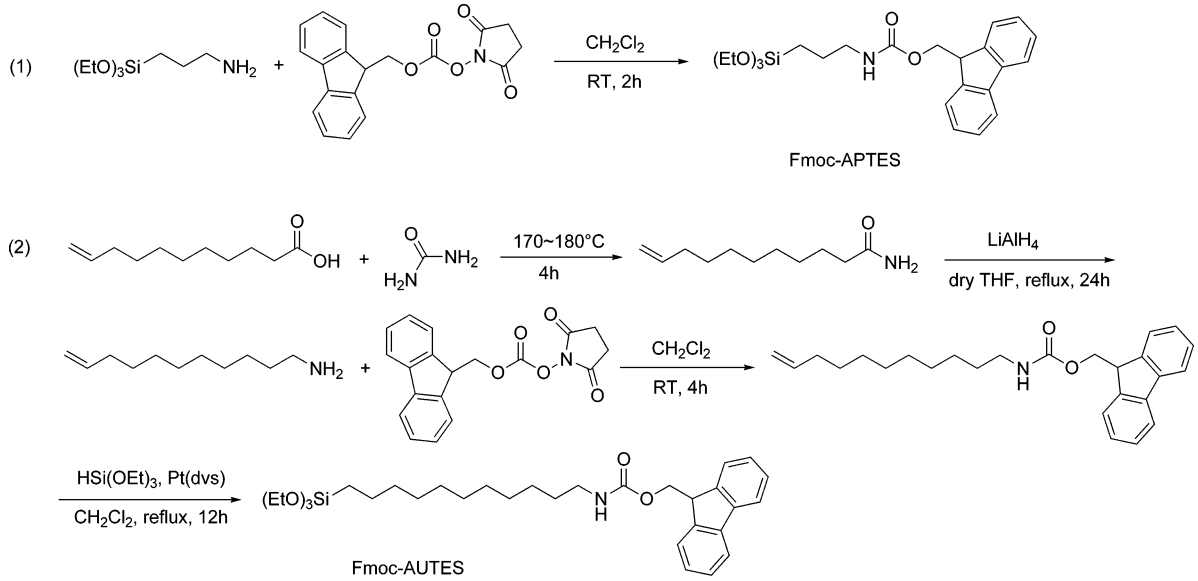

[a] Abbreviations: Fmoc, *N*-(9-fluorenylmethyloxycarbonyl); $LiAlH_4$, lithium aluminum hydride; $HSi(OEt)_3$, triethoxysilane; Pt(dvs), Platinum(0)-1,3-divinyl-1,1,3,3-tetramedisiloxane complex, 3 wt % in xylenes.

piperidine solutions could therefore be varied to study the effects on reaction rate by measuring the absorbance of the released Fmoc adducts.

Fluorescence confocal scanning laser microscopy (CSLM), in combination with fluorescent labeling, was used to study the locations of various molecules within APMS. The ability of the confocal microscope to create a thin focal plane allows an optical "slice" to be taken through the center of the APMS particle; regions of the particle outside the focal plane do not appear in the final image. This technique allows fluorescence originating from within the pores of APMS to be distinguished from fluorescence on the external surface. Using dyes that can form peptide bonds allows free amines bound to the internal pore surfaces to be distinguished from those on the external surface.

Surface Functionalization of APMS. 9-Fluorenylmethyloxycarbonyl propylcarbamate (Fmoc-propylamine) was introduced by direct reaction of (9*H*-fluorenyl)methyl 3-(triethoxysilyl)-propylcarbamate (Fmoc-APTES, Scheme 1) to silica surfaces. Other organosilanes, including (9*H*-fluorenyl)methyl 11-(triethoxysilyl)undecylcarbamate (Fmoc-AUTES), 3-aminopropyltriethoxysilane (APTES), were also studied for the comparisons. Fmoc-AUTES was selected as an immobilized functional linker on the silica due to its longer alkyl chain;[27] therefore, the incorporation of the long alkyl moiety of Fmoc-AUTES was expected to fill the pores of the silica completely. Fmoc-APTES was obtained by the reaction of APTES with *N*-(9-fluorenylmethyloxycarbonyl)oxysuccinimide (Fmoc-OSu) in high yield (90%). In contrast, Fmoc-AUTES was prepared through a series of reactions since the triethoxysilane was unavailable. Undeylenic acid was reacted with urea to give ω-undecenamide, which was further converted to 11-undecenylamine by reduction with $LiAlH_4$. Before the hydrosilation, the amine groups were protected with Fmoc. The resulting amide derivative was then hydrosilated with triethoxysilane in the presence of the Karstedt catalyst (platinum(0)-1,3-divinyl-1,1,3,3-tetramethyldisiloxane complex, $\{Pt_2((CH_2{=}CH)Me_2Si)_2O\}_3$).

In order to study the density and distribution of the incorporated functional groups, we initially prepared a series of silica samples in which different amounts of organosilanes were immobilized on the surface by varying the concentrations of the silanes during the modifications.[30] The organic moieties on the silica surface were characterized by TGA, which gave the organic contents.[21,37] TGA data for APMS-Fmoc are summarized in Table 1 (actual TGA traces can be found in the Supporting Information). Additional confirmation of the organic loadings was obtained by UV/visible spectrophotometry of the Fmoc groups. In this analysis, the Fmoc groups were cleaved from the silica framework by etching the silica in aqueous HF, and the Fmoc groups were recovered from the mixture by extraction. Absorbance of the extractant at 289 nm was then correlated with a calibration curve.[27] The results of both methods correlated closely. The slight difference between the two methods may be derived from either incomplete hydrolysis of ethoxy groups, leading to higher organosilane loadings in TGA, or incomplete recovery of Fmoc in the extraction step, leading to lower organosilane loading in UV/visible spectrophotometry. Since TGA could be accomplished more readily, it was used for the remaining calculations. There were three or four distinct weight losses in the TGA profiles that were due to loss of MeOH, organic functional groups, and dehydration of the surface hydroxyl groups.[37] It has been reported that the loading of organosilanes on the silica surface by condensation of Si−OR groups can be regarded as a Langmuir adsorption process.[21] Because the temperature was maintained at the boiling point of toluene (110 °C), the degree of surface functionalization was determined by the concentration of silanes in solution (C_{silane}) during the functionalization. The organic loadings were calculated from the TGA data using units of mole per gram of pure silica (mol/g of SiO_2). As the concentration of the organosilane increased, the loading also increased until it reached the maximum possible loading. The curves of surface loadings were

(37) Zhao, X. S.; Lu, G. Q.; Whittaker, A. K.; Millar, G. J.; Zhu, H. Y. *J. Phys. Chem. B* **1997**, *101*, 6525.

Table 1. Organic Loading and Surface Coverage of Organosilanes on APMS and Nucleosil

sample[a]	organosilane concentration (mM)	organosilane loading, Γ[b] (mmol/g SiO_2)	surface density, α (molecule/nm^{-2})	surface coverage, θ (%)
APMS-3-NH_2-4	4.2	0.730	0.400	25.26
APMS-3-NH_2-8	8.3	1.28	0.701	44.15
APMS-3-NH_2-21	21	2.01	1.10	69.55
APMS-3-NH_2-42	42	2.31	1.26	79.93
APMS-3-NH_2-63	63	2.40	1.31	83.04
APMS-3-NH_2-83	83	2.57	1.41	88.93
APMS-3-NH_2-150	150	2.58	1.42	89.27
APMS-3-Fmoc-20	20	0.445	0.244	33.46
APMS-3-Fmoc-33	33	0.554	0.303	41.65
APMS-3-Fmoc-45	45	0.645	0.353	48.50
APMS-3-Fmoc-60	60	0.737	0.403	55.41
APMS-3-Fmoc-100	100	0.891	0.488	66.99
APMS-3-Fmoc-135	135	0.988	0.541	74.29
APMS-3-Fmoc-200	200	1.11	0.608	83.53
APMS-11-Fmoc-10	10	0.128	0.0701	14.71
APMS-11-Fmoc-20	20	0.203	0.111	23.33
APMS-11-Fmoc-50	50	0.422	0.231	48.51
APMS-11-Fmoc-83	83	0.523	0.286	60.11
APMS-11-Fmoc-100	100	0.549	0.300	63.10
APMS-11-Fmoc-200	200	0.617	0.338	70.92
Nucleosil-3-Fmoc-200	200	0.553	0.772	–
Nucleosil-11-Fmoc-200	200	0.392	0.548	–
deprotected APMS-3-Fmoc-135 (6 h)	–	0.395 Fmoc– (40%) + 0.593 –NH_2 (60%)		
deprotected APMS-3-Fmoc-135 (24 h)	–	0.119 Fmoc– (12%) + 0.869 –NH_2 (88%)		

[a] Nomenclature: "APMS-*n*-R-*m*", where n = carbon atoms in organic "linker", R = functionalization, and m = organosilane concentration in loading solution. [b] Calculated from TGA data.

Table 2. Parameters Obtained from Langmuir Fitting of Loading Data for Fmoc-APTES, Fmoc-AUTES, and APTES

silanes	intercept ($1/\Gamma_{max}$)	slope ($1/\Gamma_{max}K$)	equilibrium constant, K (M^{-1})	maximum loading, Γ_{max} (mmol/g)	maximum density, α_{max} (nm^{-2})	R^2
APTES	0.351	0.003 52	100	2.85	1.56	0.99
Fmoc-APTES	0.750	0.0355	21.1	1.33	0.728	0.99
Fmoc-AUTES	1.16	0.0675	17.0	0.862	0.472	0.99

fit by the Langmuir adsorption equation (eq 1).[21]

$$\theta = \frac{\Gamma}{\Gamma_{max}} = \frac{KC_{silane}}{1 + KC_{silane}} \quad (1)$$

The equilibrium constant (K) and the maximum loading in mmol of organosilane/g of SiO_2 (Γ_{max}) were obtained from the parameters of the fitting data of surface loading by the Langmuir adsorption model. Strict application of this model would assume complete independence of adsorbate molecules, and the organosilanes in our experiments could interact with the surface and with each other. Although a more detailed description is not appropriate, use of the Langmuir model allowed quantitative comparison of data sets to be made. The loading curves of these silanes are shown in Figure 1, and the parameters calculated from the Langmuir equation are listed in Table 2. APTES achieved a saturated monolayer on the silica surface below 0.075 M, while Fmoc-APTES and Fmoc-AUTES require significantly higher concentrations (above 0.15 M). APTES also showed a much higher equilibrium constant (about 100 M^{-1}). It has been reported that there are strong interactions between hydrophilic silanols on the silica surface and APTES which contributes to the higher equilibrium constants.[21] In contrast, the equilibrium constants of Fmoc-APTES and Fmoc-AUTES were much lower (less than 25 M^{-1}), consistent with the fact that both organosilanes contain hydrophobic groups as the terminal group, which were not favorably adsorbed onto the hydrophilic silica walls. Moreover, Fmoc-AUTES has a longer alkyl chain, causing more steric hindrance to accessing the pores and resulting in a lower equilibrium constant.

The surface density of the organosilanes (α) was calculated from eq 2, where N_A is Avogadro's number and S_{BET} is the BET surface area of the porous silica in m^2/g :[21]

$$\alpha = \frac{\Gamma N_A}{S_{BET}} \times \left(\frac{\text{mol} \cdot \text{m}^2}{10^3 \text{ mmol} \cdot 10^{18} \text{ nm}^2} \right) \quad (2)$$

When the coverage of APTES on APMS was 83.0% (Table 1), its surface density was 1.31 molecules/nm^2. Consistent with the results shown above, the surface densities of Fmoc-APTES and Fmoc-AUTES were lower than this value (1.11 molecules/nm^2 at 83.5%, 0.34 molecules/nm^2 at 70.9%, respectively), due to the steric hindrance and hydrophobicities of those molecules. Finally, the theoretical maximum densities of the attached silanes were calculated from the Langmuir fitting parameter (Table 2).[21] The functional silanes can be ranked in order of increasing maximum surface densities as follows: Fmoc-AUTES (0.48 molecules/nm^2) < Fmoc-APTES (0.73 molecules/nm^2) < APTES (1.58 molecules/nm^2).

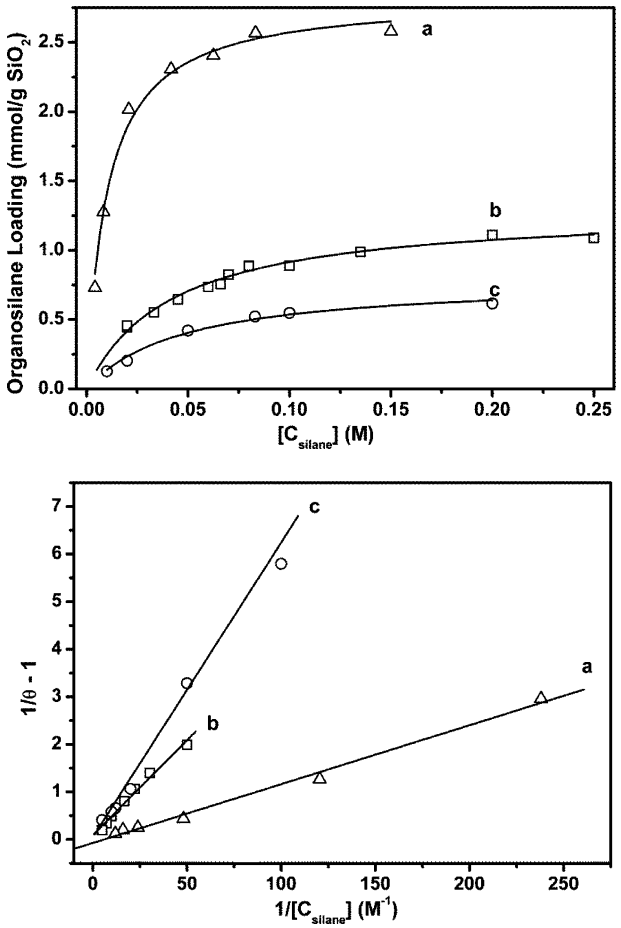

Figure 1. (Top panel) Isotherms of organosilanes loaded into APMS. (Bottom panel) Linear fits of the organosilane loadings derived from the Langmuir equation: (a) APTES; (b) Fmoc-APTES; (c) Fmoc-AUTES.

Physical Characterization of Materials. ^{29}Si MAS NMR spectra of calcined APMS before and after silation are shown in Figure 2. For the calcined APMS, the resonance centered at $\delta = -111$ ppm with two shoulders at -103 and -93 ppm was assigned to siloxane (Q^4, $Si(OSi)_4$), single silanol (Q^3, $Si(OSi)_3OH$), and geminal silanol (Q^2, $Si(OSi)_2(OH)_2$) sites.[29,37,38] The spectrum of functionalized APMS showed two additional resonances at approximately $\delta = -58$ and -67 ppm, which represented T^2 ($RSi(OSi)_2(OH)$) and T^3 ($RSi(OSi)_3$) sites, respectively. The relative amounts of each type of Si atom were calculated from the deconvolution of the spectra. The slight decreases in the number of Si atoms in Q^3 and Q^2 environments were due to the reaction of silanol groups with the organosilanes, and the presence of Si atoms in T^3 and T^2 environments in the functionalized APMS samples further indicated the existence of the covalent linkage between the organic moieties and silica walls.

Data from the characterization of the porous samples by N_2 physisorption are shown in Table 3. The isotherm of unmodified APMS exhibited a Type IV isotherm[4,5,39] with a point of inflection at approximately $p/p_0 = 0.2-0.4$, consistent with the presence of mesopores. This sample had the large surface area (1177 m^2/g) and pore volume (0.625 cm^3/g) characteristic of mesoporous materials.[4] As expected, the introduction of the organic moieties led to a decrease in pore diameter, surface area, and pore volume. The functionalized APMS samples increasingly showed characteristics of Type I isotherms as a function of the degree of silation, indicating that the pore diameter had decreased. Calculation of the average pore diameters of the samples indicated a decrease from 30 Å for unmodified APMS to 21 Å for APMS-3-Fmoc-135. APMS-3-Fmoc-200 did not even show the presence of any pores, since they were completely filled with organic moieties. The changes in measured pore diameter were consistent with the surface area (5.72 m^2/g) and pore volume (0.0118 m^2/g) for this sample. It is also worth noting that the sharpness of the pore size distribution decreased as the degree of silation increased, which is indicative of inhomogeneous pore filling.[40,41] A similar decrease in the porosity of APMS was observed upon binding of Fmoc-AUTES, although the decreases occurred at different organic loadings. An examination of the data in Table 1 shows that APMS-3-Fmoc-45 and APMS-11-Fmoc-50 have approximately the same surface areas (519 and 500 m^2/g, respectively), while their organic loadings are different (0.645 vs 0.422 mmol of organosilane/g of SiO_2). A more dramatic comparison is APMS-3-Fmoc-200 and APMS-11-Fmoc-200, which have surface areas of 5.72 and 32.7 m^2/g but loadings of 1.11 and 0.617 mmol/g. These differences can be attributed to the longer chain of Fmoc-AUTES (23 Å, almost twice that of Fmoc-APTES), which can occupy the available pore space more completely. Finally, a commercially available material, Nucleosil-50, was used for comparison. This material had a very broad pore size distribution with an average pore diameter of approximately 80 Å. Nucleosil could be easily modified by reaction with either Fmoc-APTES or Fmoc-AUTES, which is indicated by the fact that Nucleosil-3-Fmoc-200 and Nucleosil-11-Fmoc-200 showed higher surface densities than their APMS-based counterparts at similar organosilane loadings. Additionally, at a concentration of organosilane in solution that essentially resulted in pore closure in APMS (200 mM), Nucleosil still retained 75% of its surface area and pore volume

Table 3. Physical Properties of Selected Samples from Table 1

sample	surface area (m^2/g)	pore volume (cm^3/g)	avg pore diameter (Å)
unmodified APMS	1180	0.625	30
APMS-3-Fmoc-20	686	0.315	23
APMS-3-Fmoc-33	624	0.274	23
APMS-3-Fmoc-45	519	0.248	24
APMS-3-Fmoc-60	444	0.209	22
APMS-3-Fmoc-100	331	0.144	22
APMS-3-Fmoc-135	88.3	0.0489	21
APMS-3-Fmoc-200	5.72	0.0118	<20
APMS-11-Fmoc-50	500	0.231	23
APMS-11-Fmoc-200	32.7	0.061	<20
unmodified Nucleosil	431	0.911	80
Nucleosil-3-Fmoc-200	332	0.641	66
Nucleosil-11-Fmoc-200	315	0.671	67
deprotected APMS-3-Fmoc-135 (6 h)	691	0.300	25
deprotected APMS-3-Fmoc-135 (24 h)	764	0.378	26

(38) Chong, A. S. M.; Zhao, X. S. *J. Phys. Chem. B* **2003**, *107*, 12650.
(39) Sing, K. S. W.; Everett, D. H.; Haul, R. A. W.; Moscou, L.; Pierotti, R. A.; Rouquerol, J.; Siemieniewska, T. *Pure Appl. Chem.* **1985**, *57*, 603.
(40) Luan, Z.; Xu, J.; He, H.; Klinowski, J.; Kevan, L. *J. Phys. Chem. B* **1996**, *100*, 19595.
(41) Luan, Z.; He, H.; Zhou, W.; Cheng, C. F.; Klinowski, J. *J. Chem. Soc., Faraday Trans.* **1995**, *91*, 2955.

Scheme 2. Fmoc Deprotection Reaction, Synthesis of Fmoc-Functionalized Silicas, and Deprotection Strategy

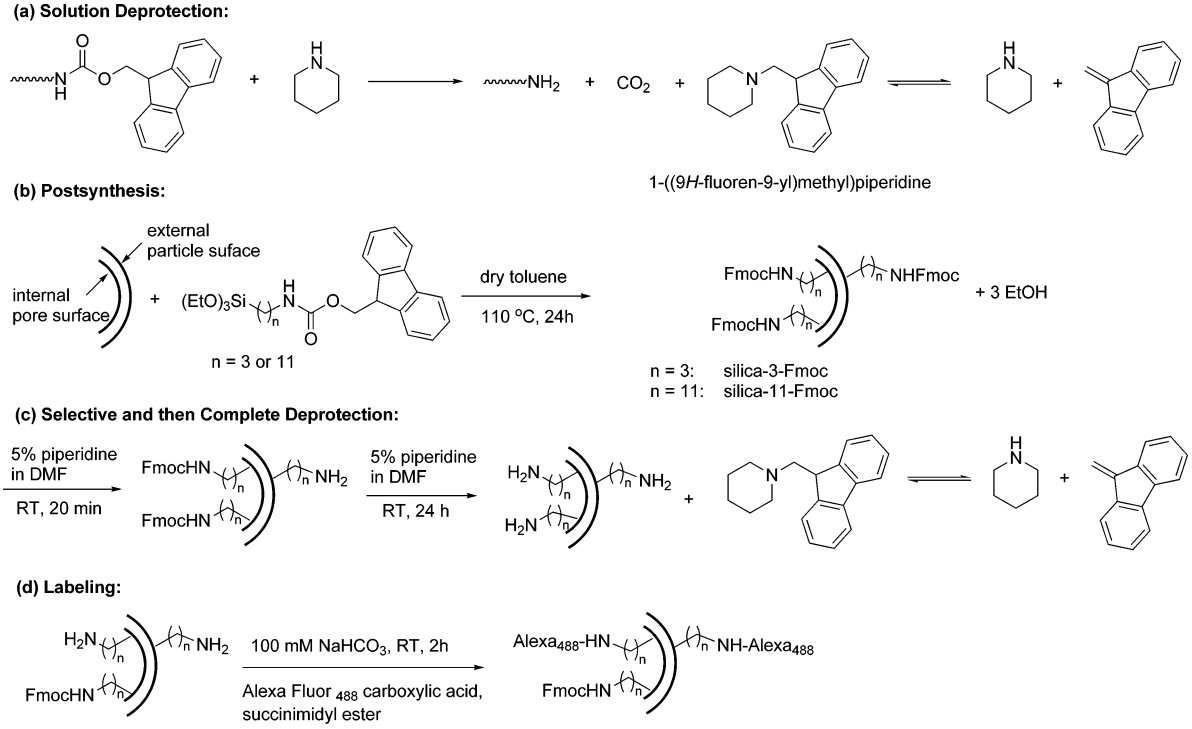

for both Fmoc-APTES and Fmoc-AUTES, which is consistent with the broad pore size distribution and therefore the number of large pores within this material.

Nitrogen physisorption data on the deprotected materials were also obtained. It can be clearly observed that exposure of the Fmoc-organosilane modified solids to a solution of 5% piperidine in DMF led to a significant increase in pore diameter, surface area, and pore volume. Based on TGA experiments, 60% of the Fmoc groups of APMS-3-Fmoc-135 were removed after 6 h, and 88% were removed after 24 h. A drastic increase in surface area (from 88.3 to 764 m^2/g) and pore volume (from 0.0489 to 0.378 cm^3/g) indicated the blocked pores were "reopened" by the cleavage of bulky Fmoc groups from Fmoc-modified silica. Importantly, the isotherm of deprotected APMS-3-Fmoc-135 reverted to Type IV from Type I, indicating that the mesoporous properties of the solid had been regenerated, with a measured pore diameter of 26 Å. The increase of 5 Å in pore diameter after the deprotection was consistent with the difference in molecular diameter between the Fmoc-aminopropyl and free-aminopropyl moieties.

Deprotection Studies. The deprotection reaction of Fmoc groups confined in pores with diameters approaching molecular diameters, as in APMS, is a diffusion-controlled process.[6] In this case, piperidine first diffuses into the pores to reach the Fmoc-aminopropyl moieties, where it reacts quickly to form an Fmoc-piperidine adduct, 1-(9*H*-fluoren-9-ylmethyl)piperidine, which then diffuses out of the pores. The reaction rate is thus determined by several factors including the chemical kinetics of surface deprotecting reaction, the diffusivity of the reagent or product in the solvent, the tortuosity factor, and porosity of the silica particles.[42]

The mechanism of the Fmoc deprotection reaction is shown in Scheme 2.[36,43] The Fmoc-piperidine adduct strongly absorbs in the UV region (λ_{max} = 273, 289, and 300 nm) and has been used as a marker of amine deprotection in other studies.[36] To study the kinetics of amine deprotection in porous solids, the reaction was monitored by taking solution aliquots and measuring the change in absorbance at 289 nm. The release rates of the Fmoc-adducts were expressed as the percentage of Fmoc groups released, determined from the Fmoc-organosilane loadings in Table 1, as a function of time. An example of this plot is shown in Figure 3. Several empirical models were examined for their ability to fit the sigmoidal curves shown in this figure.[24] The best results were obtained by using the Hill equation, which is also known as the variable slope sigmoid and is frequently used to model pharmacological phenomena.[24,44] This equation is used for many physical, chemical, biological, and environmental processes that are driven by two different mechanisms: diffusion and chemical or biological reaction.[44,45] The Hill equation is shown below (eq 3):

$$Y(t) = Y_0 + \frac{Y_{max}}{1 + (t_{1/2}/t)^H} \quad (3)$$

where $Y(t)$ is the cumulative amount of the Fmoc-adduct at time t, Y_0 is the initial amount of Fmoc-adduct, Y_{max} is the maximum amount of Fmoc-adduct released, $t_{1/2}$ is the time at which $Y(t)$ reaches $Y_{max}/2$, and H is the Hill coefficient, which gives the slope of the sigmoidal curve at $t_{1/2}$. The plots of Fmoc-adduct release for modified APMS can be divided into three parts—

(42) Andrade, J., J. S.; Street, D. A.; Shibusa, Y.; Havlin, S.; Stanley, H. E. *Phys. Rev. E* **1997**, *55*, 772.

(43) Chan, W. C.; White, P. D. *Fmoc Solid Phase Peptide Synthesis: A Practical Approach*; Oxford University Press: Oxford, 2000.

(44) Lombardo, T.; Ionescu, A.; Lefevre, R. A.; Chabas, A.; Ausset, P.; Cachier, H. *Atmos. Environ.* **2005**, *39*, 989.

(45) Calace, N.; Nardi, E.; Petronio, B. M.; Pietroletti, M. *Environ. Pollut.* **2002**, *118*, 315.

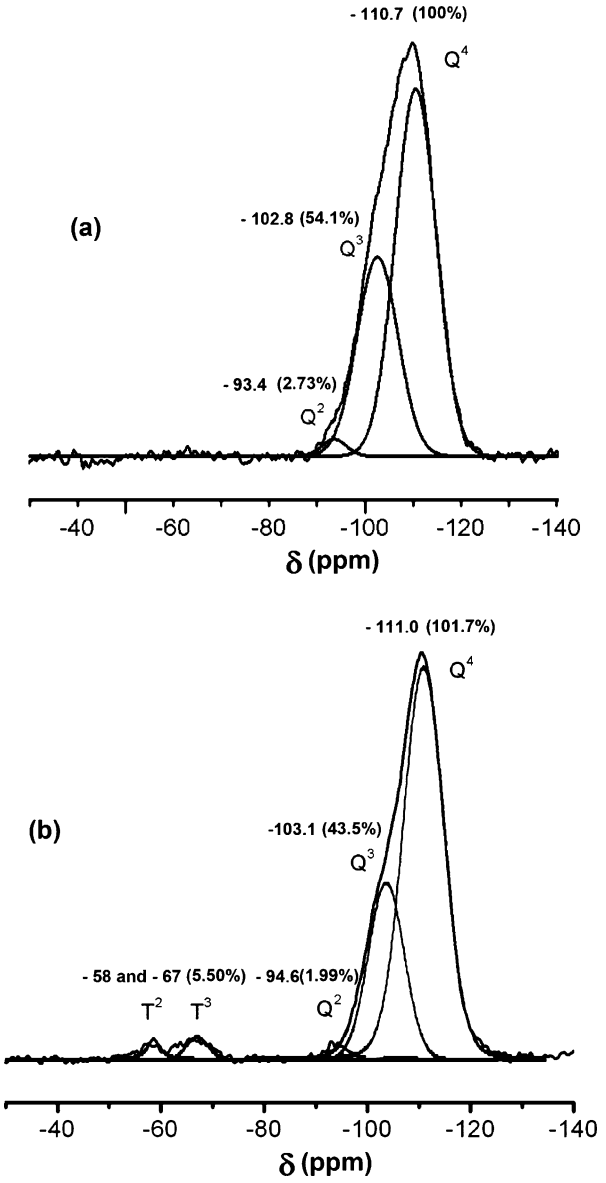

Figure 2. ^{29}Si MAS NMR of (a) unmodified APMS and (b) APMS-3-Fmoc-135. Chemical shifts from deconvolution of the spectra are marked, and relative peak areas normalized to the area of the Q^4 peak in (a) are given in parentheses.

the lag phase, the burst phase, and the saturated phase (Figure 3)—and described by the parameters in eq 3.[24] In the lag phase, the release curve starts with a small value (Y_0) and a slope of almost zero, slowly increasing at the beginning ($t < t_{lag}$). The length of the lag phase (t_{lag}) depends on the intrinsic characteristics of the heterogeneous reaction on the exterior surface of the silica beads. In the burst phase, the slope of the release curve increases to a maximum value (K_m) and then slowly decreases again until it is effectively horizontal. The saturated phase was expected to appear when $Y(t)$ reaches more than 90% of Y_{max}.[24] The first derivative of the release curve (eq 4, Figure 3b) illustrates the rate of release; the time at maximum release rate (t_m) can be found from this equation, and it can also be used to determine the rate at t_{lag} (K_{lag}).

$$K = \frac{\partial Y(t)}{\partial t} = Y_{max} H \frac{t^{H-1} t_{1/2}^{H}}{(t_{1/2}^{H} + t^{H})^2} \qquad (4)$$

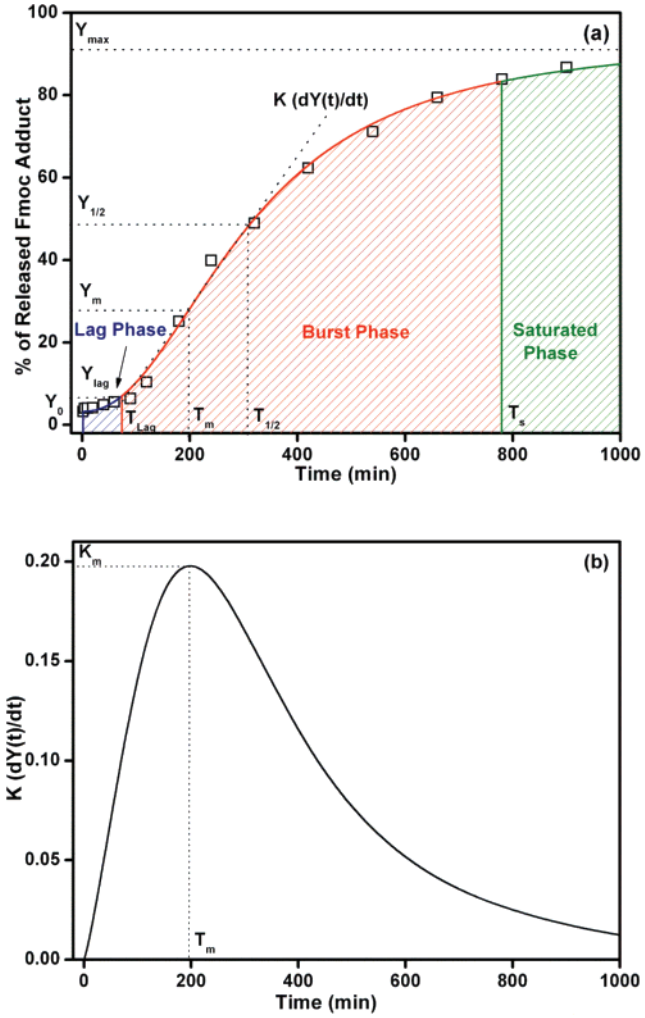

Figure 3. Cumulative amount of Fmoc-piperidine adduct released from APMS-3-Fmoc-135 in a DMF solution containing 5% piperidine at room temperature. The three phases of the process (lag, burst, and saturation) were characterized as described in the text. The first derivative of the curve is shown in (b).

The length of the lag phase (t_{lag}) can be obtained from eq 5.

$$t_{lag} = t_m - \frac{Y_m - Y_0}{K_m} \qquad (5)$$

Table 4 shows the values of selected Hill parameters, all of which were obtained by fitting Fmoc-adduct release curves for various samples to eq 3. The correlation coefficients (R^2) were in all cases greater than 0.995.

In organic synthesis, *N*-Fmoc groups are typically removed by treatment with 20−50% v/v piperidine in DMF. Under these conditions and in solution, the Fmoc groups can be quickly cleaved to afford the free amine and dibenzofulvene in less than 1 min. Lower concentrations of piperidine in DMF (2%, 5%, and 10%) have been studied in an attempt to kinetically control the deprotection reaction.[36] Although $t_{1/2}$ for deprotection of Fmoc-amino derivatives in solution varied with the structure of each compound, the approximate value of $t_{1/2}$ for the deprotection of Fmoc-amino acid in 20% piperidine DMF solution at room temperature was only 6 s. Even in 5% piperidine, $t_{1/2}$ was only 20 s.[36] However, the half-lives for the heterogeneous system are very different. In this case, $t_{1/2}$ in 20%

Table 4. Parameters from Eqs 3 and 5 for the Release of Fmoc−Piperidine Adducts under Various Conditions[a]

sample	temp (°C)	piperidine (vol %)	Y_{max} (%)	$T_{1/2}$ (min)	K_m	T_m (min)	K_{lag}	T_{lag} (min)	Y_{lag} (%)
APMS-3-Fmoc-100	25	2	89.96 ± 1.29	233.8 ± 4.4	0.302	175.6	0.0766	81.74	6.26
	25	5	82.41 ± 2.07	129.1 ± 5.6	0.420	76.38	0.176	26.29	4.63
	25	10	81.57 ± 1.50	105.7 ± 2.8	0.500	59.90	0.278	19.92	5.54
	25	20	73.93 ± 1.02	95.42 ± 1.92	0.509	56.57	0.359	19.53	7.02
	25	40	67.01 ± 1.17	94.93 ± 1.83	0.460	57.24	0.420	19.22	8.07
	30	2	89.01 ± 1.48	106.9 ± 2.3	0.658	81.53	0.184	38.16	7.01
	30	5	87.54 ± 1.60	72.94 ± 2.01	0.783	42.62	0.416	14.39	5.99
	40	2	94.19 ± 0.77	39.18 ± 0.46	1.90	30.01	0.576	14.00	8.06
	40	5	90.03 ± 1.54	24.35 ± 0.61	2.67	17.16	0.984	7.093	6.98
APMS-3-Fmoc-33	25	5	–	1.92[b]	–	–	–	–	–
APMS-3-Fmoc-45	25	5	–	4.03[b]	–	–	–	–	–
APMS-3-Fmoc-60	25	5	82.16 ± 1.55	68.78 ± 2.04	0.800	42.65	0.708	15.37	10.9
APMS-3-Fmoc-100	25	5	81.03 ± 2.70	129.1 ± 5.6	0.412	75.81	0.199	26.18	5.22
APMS-3-Fmoc-135	25	5	90.96 ± 2.25	312.0 ± 9.8	0.198	198.1	0.0946	73.65	6.97
APMS-3-Fmoc-200	25	5	94.30 ± 6.21	591.1 ± 35.5	0.133	465.6	0.0431	231.9	9.99
APMS-11-Fmoc-50	25	5	–	16.18[b]	–	–	–	–	–
APMS-11-Fmoc-200	25	5	82.50 ± 2.11	128.3 ± 5.5	0.392	43.75	1.47	8.293	12.2
Nucleosil-3-Fmoc-200	25	5	82.60 ± 3.81	33.28 ± 2.49	1.62	19.95	2.77	6.629	18.4
Nucleosil-11-Fmoc-200	25	5	87.54 ± 2.33	45.45 ± 1.82	1.17	19.09	2.48	4.405	10.9

[a] A complete list of parameters may be found in the Supporting Information. [b] $T_{1/2}$ values for samples with low organosilane loadings were estimated directly from the release curves.

piperidine solution at room temperature is 95.4 min and is 234 min in 2% piperidine solution. These significant differences are evidence of the presence of diffusion constraints during the deprotection reaction. In the absence of piperidine, APMS-Fmoc exhibited less than 3% Fmoc release in DMF solution over a period of 24 h (Figure 4a), indicating that Fmoc-groups are chemically stable. As expected, higher concentrations of piperidine resulted in lower values of $t_{1/2}$. Even in 40% piperidine solution, however, $t_{1/2}$ is still 94.9 min. The effects of three different temperatures (25, 30, and 40 °C) on $t_{1/2}$ were also studied. As shown in Figure 4b and Table 4, $t_{1/2}$ decreased remarkably as temperature increased for piperidine concentrations of both 2 and 5%. This can be explained by the accelerated diffusion of the piperidine and Fmoc-piperidine adduct through the pores of silica at higher temperatures. Higher temperatures also increased the rate of the Fmoc-deprotection reaction itself, resulting in a smaller value of $t_{1/2}$.

Data from the lag and burst phases of the release curves (Table 4 and Figure 5) provide interesting information about the deprotection reaction on this porous substrate. On flat surfaces, heterogeneous deprotection reactions are said to involve sequential steps: the reagent diffuses to the surface and quickly reacts to form products, which then diffuse away.[46,47] Thus, as long as the concentration of piperidine is sufficiently high, the surface reaction should take place quickly and t_{lag} should be short or nonexistent. Indeed, APMS-3-Fmoc-33 and -45, with relatively low organosilane loadings and open pores, showed hyperbolic rather than sigmoidal Fmoc-adduct release curves, and eqs 3−5 could not be applied effectively. At intermediate organosilane loadings, the fact that t_{lag} exists and increases with loading indicates that diffusion of piperidine and the Fmoc−piperidine adduct within the pores is hindered. This must be due to inhomogeneity in the distribution of Fmoc within the pores, consistent with other reports indicating that higher densities of functional group are located on the exterior surfaces and near the openings of mesoporous channels rather than in

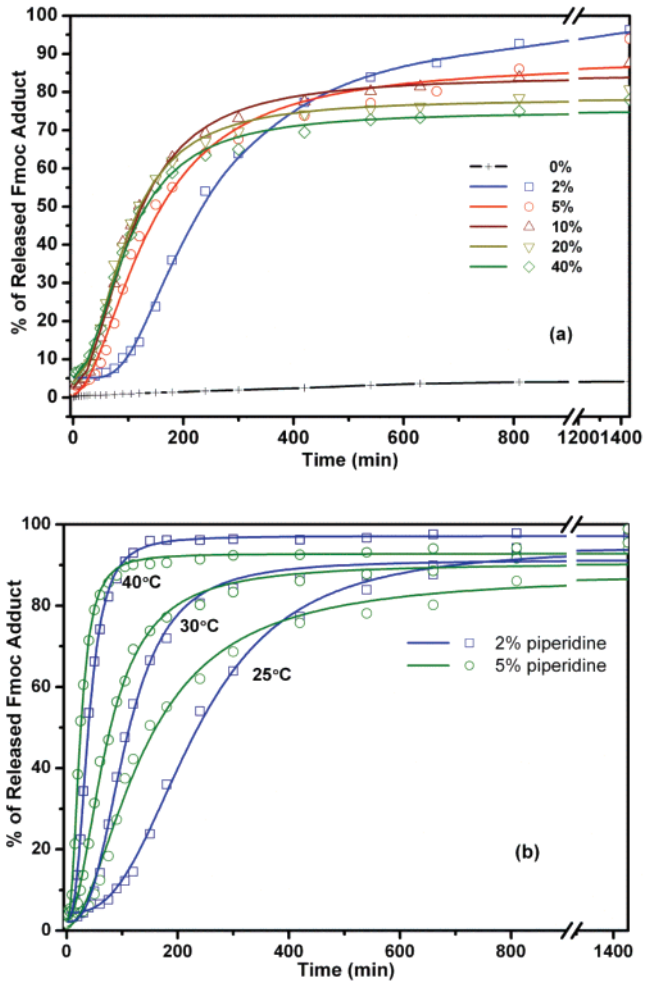

Figure 4. Cumulative release of the Fmoc−piperidine adduct from APMS-3-Fmoc-100 in (a) DMF solutions containing piperidine concentrations between 0 and 40% at room temperature and in (b) DMF solutions containing 2 or 5% piperidine at temperatures between 25 and 40 °C.

(46) Aris, R. *The Mathematical Theory of Diffusion and Reaction in Permeable Catalysts*; Clarendon: Oxford, 1975.
(47) Cussler, E. L. *Diffusion: Mass Transfer in Fluid Systems*, 2nd ed.; Cambridge University Press: Cambridge, 1997.

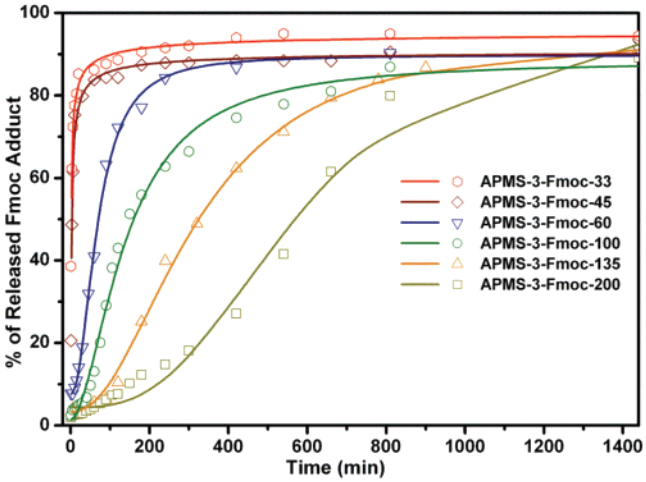

Figure 5. Cumulative release of the Fmoc−piperidine adduct from various APMS-3-Fmoc samples in a solution of DMF containing 5% piperidine at room temperature.

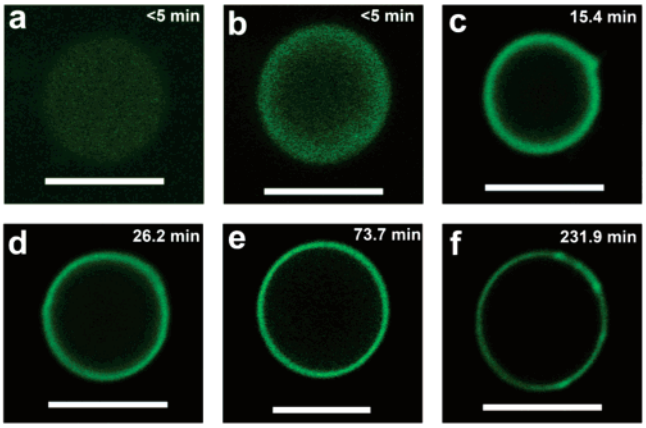

Figure 6. Fluorescence CSLM images of deprotected APMS-3-Fmoc-*n* samples with Alexa 488 (a fluorescent green dye) covalently bound to the free amine, where n = (a) 33, (b) 45, (c) 60, (d) 100, (e) 135, and (f) 200. Samples were deprotected in 5% piperidine in DMF at room temperature for 40 min. The t_{lag} for each sample (see Table 4) is listed in the top right corner of each image (bar = 5 μm).

the porous interior.[21,33,34] One might expect that APMS-3-Fmoc-200, which contained pores that were essentially completely filled, would have both an unusually large t_{lag} and a relatively short burst phase, since penetration of piperidine to the porous interior of the particles is continually hindered by organosilane groups. As anticipated, these features are found for the release curve of APMS-3-Fmoc-200. After the pore entrances are opened during the lag phase, the piperidine is able to access the Fmoc-organosilane groups within the pores. Since the majority (over 99.9%) of the total surface area of APMS is located within the pores, as long as the concentration of piperidine is sufficiently high the release rate should increase dramatically after the pore entrances are cleared. It is also found that increased organosilane surface densities should produce longer burst phases, reflected in a release curve with a broader shape and a longer t_m. The value of the maximum rate, K_m, also decreases as the organosilane surface increases, due to hindered molecular diffusion within pores of materials with higher organosilane loadings.

We also performed studies varying the concentration of piperidine and the temperature for a given substrate with an intermediate organosilane loading (APMS-3-Fmoc-100). Decreasing the piperidine concentration from 5 to 2% caused a dramatic increase in t_{lag} and t_m, with a decrease in the rate of the Fmoc−piperidine adduct released (K_m). Conversely, increasing the concentration of piperidine from 5 to 10% had the opposite effects; increasing the concentration further did not produce a dramatically different result. This provides support for the results described above, since it appears that as long as the concentration of piperidine in the solution is high enough that diffusion to the surface is not hindered (i.e., there is always piperidine available for deprotection), the limiting factor in the rate of deprotection is the access of the piperidine to the internal pore surface. Thus, K_m values are similar at piperidine concentrations of 5−40%. In order to have the organosilane loading be the rate-limiting effect, concentrations of at least 5% should be used. Similarly, increasing the temperature of the system had a significant effect on t_{lag}, t_m, and K_m, indicating that molecular diffusion of piperidine both to the solid surface and through the pores and the rate of the deprotection reaction itself are all important to the overall rate of release. Significantly, K_m was approximately 5 times larger at 40 °C than at 25 °C.

Visual Analysis of Deprotection by Confocal Microscopy. Effective use of the data above requires experimental demonstration that the deprotected amines can be refunctionalized, for example, through peptide bond formation, to allow APMS to be differentially modified. Based on the above results, we theorized that t_{lag} could be a controlling factor in this differential modification. Fluorescence confocal scanning laser microscopy (CSLM), combined with fluorescent labeling, was used to locate deprotected propylamine moieties with APMS-Fmoc samples. Our initial studies used a constant concentration of 5% piperidine in DMF for 40 min for the deprotection of various APMS-3-Fmoc-modified materials. The fluorescent dye Alexa Fluor 488 (λ_{max} = 488 nm), as the carboxylate succinimidyl ester, was bound to any free amines present after the deprotection step, providing the location of free amines. Although the molecular diameter of the dye is larger than piperidine or its derivative, the labeling time (16 h) was long enough to allow the dye to penetrate the pores of the solid. CSLM was then used to select an optical slice located at the center of a particle. As shown in Figure 6, the interiors of most of the particles appeared darker than the exteriors, and the particles appeared as rings, indicating that there were fewer labeled propylamine moieties within the pores than on the external particle surface. The brightness and thickness of the ring corresponded to the number of deprotected amine groups and the penetrating depth of the piperidine during the deprotection, respectively. APMS-3-Fmoc-135 and APMS-3-Fmoc-200 showed thin, well-defined rings, indicating that the deprotection reaction was restricted mainly to the external particle surface even after 40 min. As demonstrated above, the t_{lag} for these materials (74 and 232 min, respectively) is longer than the deprotection time (40 min), and less than 5% of the total number of Fmoc groups (those located on the external surface) were deprotected. The lack of homogeneity in the CSLM image of APMS-3-Fmoc-200 lends support to the idea that the groups are not distributed homogeneously on the external surface. APMS-3-Fmoc-100 exhibited a clearly defined but slightly wider ring. For this material, t_{lag} is approximately 26 min but t_m is 76 min, so that although the groups near the pore entrances have been deprotected, the rate of Fmoc release

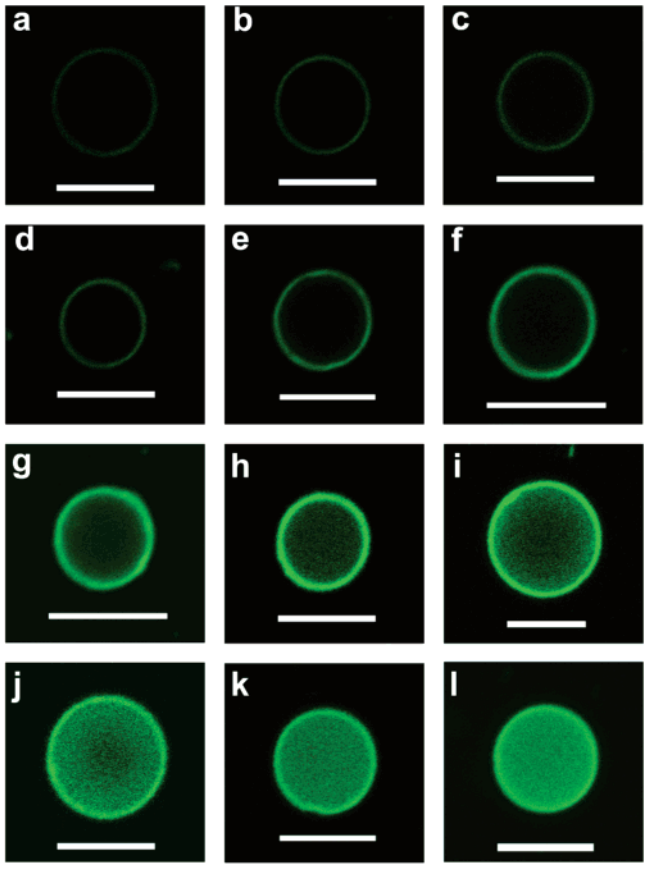

Figure 7. Fluorescence CSLM images of deprotected APMS-3-Fmoc-135. Samples were deprotected in 5% piperidine in DMF at room temperature for various times: (a) 5, (b) 10, (c) 20, (d) 40, (e) 60, (f) 90, (g) 120, (h) 240, (i) 360, (j) 540, (k) 900, and (l) 1400 min. For this sample, t_{lag} = 74 min, t_m = 198 min (bar = 5 μm).

has just begun to increase. Since the t_{lag} has been exceeded, the groups within the pores have begun to be deprotected. As expected the samples with smaller values of t_{lag} and t_m show distinct penetration of the dye to the interior of the particle, with APMS-3-Fmoc-45 and APMS-3-Fmoc-33 showing essentially complete deprotection and dye penetration. Interestingly, these samples also showed the dimmest images, since the total number of free amines and therefore dye molecules within the sample was low.

We then performed experiments on a single sample with a relatively large value of t_{lag} (APMS-3-Fmoc-135), attempting to control its degree of deprotection by varying its time of exposure to 5% piperidine (Figure 7). For this sample, t_{lag} is 74 min, and the deprotection time was varied from 5 to 1440 min. Most of the images showed a clearly defined ring. When the deprotection time was less than t_{lag}, the images consistently showed a more clearly defined ring, and the brightness of the ring increased with time. When the deprotection time became longer than t_{lag}, diffusion of the piperidine within the pores led to the broadening and brightening of the ring, although a rapid increase in dye penetration within the interior did not occur until after the deprotection time exceeded t_m (198 min). Even at t_m, however, a calculation using eq 3 and data from Table 4 indicated that only 36% of the amines were deprotected by the time t_m was reached; at 360 min, 56% of the amines were deprotected, reflected by the brightness of the images. Figure 5 indicates that the cumulative amount of released Fmoc-adduct

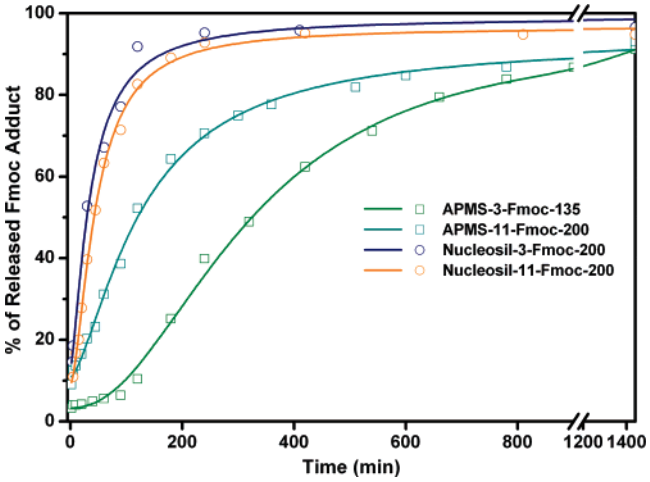

Figure 8. Cumulative release of the Fmoc−piperidine adduct from Nucleosil-3-Fmoc-200, Nucleosil-11-Fmoc-200, APMS-3-Fmoc-135, and APMS-11-Fmoc-200 in DMF solution containing 5% piperidine at room temperature.

increased almost linearly as the function of deprotection time in the burst phase. After APMS-3-Fmoc-135 was exposed to 5% piperidine for 24 h, all of the internal and external Fmoc-propylamine moieties were completely deprotected.

Comparative Release Studies on Related Materials. As discussed earlier, several factors, such as the pore diameter and organosilane loading of the solids, significantly influenced the release rate of the Fmoc-adduct. To clearly understand these factors, we compared several Nucleosil and APMS samples modified with 3-carbon and 11-carbon alkyl chains. Not included in the figure are the data for APMS-3-Fmoc-200 due to concerns with the inhomogeneous distribution of amines in this sample (Figure 6) and the fact that it was less effectively fitted to the Hill equation (Figure 5). For comparison, APMS-3-Fmoc-135 was used instead. The release curves of the Fmoc-piperidine adduct from these samples in DMF containing 5% piperidine at room temperature are shown in Figure 8. It is apparent that the release curves of samples other than APMS-3-Fmoc-135 are more like hyperbolic plots, although they still fit well to the Hill equation (correlation coefficients in all cases were greater than 0.99), and had extremely small values of t_{lag}. For a given organosilane loading, Nucleosil and APMS can be ranked in order of increasing $t_{1/2}$ as Nucleosil-3-Fmoc-200 < Nucleosil-11-Fmoc-200 < APMS-11-Fmoc-200 < APMS-3-Fmoc-135, which is consistent with the relative pore sizes of these materials. It was previously shown that, for higher organosilane loadings, the diffusion of the reagents within the pores is the rate-determining step; therefore, materials with larger pore diameters and surface areas show faster diffusion rates and faster rates of adduct release. Finally, the fluorescence CSLM images of these samples after deprotection with 5% piperidine at room temperature for a moderate time (40 min) as well as after exhaustive deprotection (24 h) are shown in Figure 9. As expected, Nucleosil-3-Fmoc-200 and Nucleosil-11-Fmoc-200 (t_{lag} = 6.6 and 4.4 min, respectively) did not show a clearly defined ring after 40 min deprotection time, since the percentage of free amines in each material is 64 and 48%. APMS-3-Fmoc-135 (t_{lag} = 74 min), with only 4.3% free amine after 40 min, shows only a thin, dim ring. APMS-11-Fmoc-200 might be expected to show a more homogeneous dye distribution, since t_{lag} (8.3 min) is significantly lower than the deprotection time.

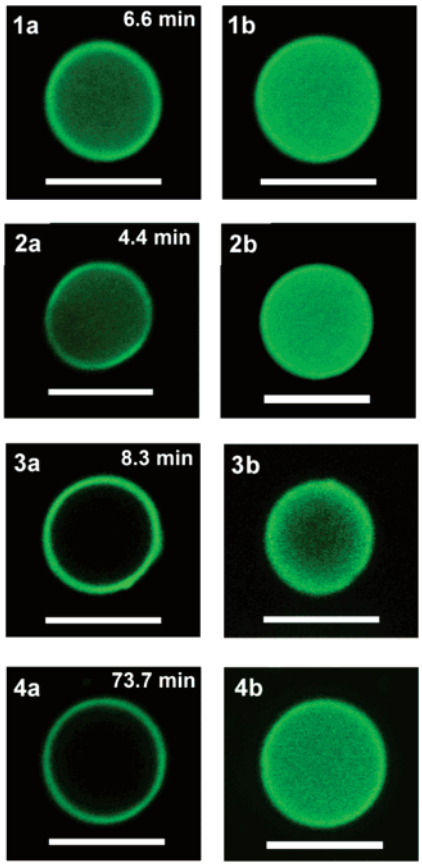

Figure 9. Fluorescence CSLM of deprotected samples with Alexa-488 bound to the free amine: (1) Nucleosil-3-Fmoc-200, (2) Nucleosil-11-Fmoc-200, (3) APMS-11-Fmoc-200, and (4) APMS-3-Fmoc-135. Samples were deprotected in 5% piperidine in DMF at room temperature for (a, left column) 40 min and (b, right column) 24 h. The t_{lag} for each sample is listed in the top right corner of the images in column a (bar = 5 μm). .

However, the ring is thicker and brighter than that for APMS-3-Fmoc-135, indicating the internal deprotection has begun, and eq 3 shows that in fact only 23% of the total amines are deprotected by this time.

Examples of Applications of Selectively Modified APMS. Based on these experiments it is possible to envision the use of selectively modified APMS in several applications, particularly drug delivery and biomolecular affinity binding. For example, in other studies we have modified the external surface of APMS with tetraethylene glycol (TEG), which enhanced the ability of APMS to penetrate the cell membranes of malignant mesotheliomas in vitro and epithelial cells in vivo.[48] This is consistent with many other studies showing that polyethylene glycol modification enhances uptake of chemotherapeutic agents.[49,50] The rapid uptake of the APMS particles led to further experiments in which TEG-modified APMS was loaded with a chemotherapeutic agent, thus using APMS as a drug delivery vehicle.[51] We are currently performing additional studies using TEG-modified APMS to enhance transfection of DNA plasmids and shRNA fragments. Although the modification methods are slightly different, the studies described in this article provide the quantitative basis for subsequent use of selectively modified APMS.

Conclusions

This study has illustrated a new and simple strategy by which the functional groups within the pores or on the surfaces of the mesoporous silica can be selectively activated for subsequent modification. The surface functionalization of APMS and Nucleosil with two Fmoc-modified organosilanes has been studied in detail. The number of organosilane groups that could be loaded onto the mesoporous surface was mainly determined by the concentration of the organosilane solution, the size and properties of the organosilane, and the physical properties of the mesoporous silica (density of free silanol groups, surface area, pore volume, and pore diameter). Under some conditions, the pores of the solid were completely filled by the Fmoc-protected organosilanes. These blocked pores could be "re-opened" by the cleavage of sterically hindered Fmoc groups from Fmoc-amino by using a solution of piperidine in DMF. UV/visible spectroscopy was used to study the release rate of an the Fmoc−piperidine adduct following organosilane deprotection, and the data were fit to the Hill equation. The rate of deprotection was influenced by the concentration and temperature of the piperidine solution, the organosilane loading and distribution within the solid, and the physical properties of the solid. The parameters from the Hill equation, particularly t_{lag}, t_m, and K_m, were used to design a process by which the internal and external organosilanes could be differentially modified. Fluorescence CSLM was used to visualize this process by labeling deprotected amines with fluorescent dyes. For example, when t_{lag} was greater than the deprotection time, the external organosilanes were selectively deprotected, allowing the location of surface functionalization to be precisely controlled. Current applications of this research in our laboratory include the selective attachment of peptides and polymers to the external surface of APMS, along with the modification of the pores for exchange of other molecules.

Acknowledgment. The authors wish to thank Prof. Doug Taatjes for assistance in obtaining confocal images and Professors Jose Madalengoitia and Martin Case for useful discussions. This work was funded in part by J. M. Huber, Inc.

Supporting Information Available: Tabulated TGA, and UV/visible data and associated spectra, ^{29}Si MAS NMR, FTIR, and powder XRD spectra, N_2 physisorption isotherms, and pore size distributions. This material is available free of charge via the Internet at http://pubs.acs.org.

JA070598B

(48) Blumen, S. R.; Cheng, K.; Ramos-Nino, M.; Taatjes, D.; Weiss, D.; Landry, C. C.; Mossman, B. T. *Am. J. Resp. Cell Mol. Biol* **2007**, *36*, 333.
(49) Mossman, B. T.; Marsh, J. P.; Hardwick, D.; Gilbert, R.; Hill, S.; Sesko, A.; Shatos, M.; Doherty, J.; Weller, A.; Bergeron, M. J. *Free Rad. Biol. Med.* **1986**, *2*, 335.
(50) Veronese, F. M.; Schiavon, O.; Pasut, G.; Mendichi, R.; Andersson, L.; Tsirk, A.; Ford, J.; Wu, G.; Kneller, S.; Davies, J.; Duncan, R. *Bioconj. Chem.* **2005**, *16*, 775.
(51) Blumen, S. R.; Cheng, K.; MacPherson, M.; Ramos-Nino, M. E.; James, T. A.; Taatjes, D. J.; Landry, C. C.; Mossman, B. T. *Cancer Res.*, submitted.